Journal of Applied Polymer Science

Structure and Rheology of Polyethylene/Imidazolium-Based Montmorillonite Nanocomposites

P. Médéric,[1] L. Le Pluart,[2] T. Aubry,[1] P.-J. Madec[2]

[1]LIMATB Equipe Rhéologie, UEB, Université de Bretagne Occidentale, 6 Avenue Victor Le Gorgeu, CS 93837, 29238 Brest cedex 3, France

[2]Laboratoire de Chimie Moléculaire et Thioorganique, UMR CNRS 6507, INC3M, FR 3038, ENSICAEN & Université de Caen, 14050 Caen, France

Correspondence to: L. Le Pluart (E-mail: loic.le_pluart@ensicaen.fr)

ABSTRACT: In this study, nanocomposites based on linear low density polyethylene (PE) and organomodified montmorillonites (MMTs) have been processed without adding any other polar compatibilizer such as maleic anhydride grafted PE. We evidence the beneficial effect on the state of dispersion of an imidazolium-based MMT compared to traditional commercial organoclays, one of which being its alkylammonium equivalent. Transmission electron microscopy observations and melt rheology are used to characterize the state of dispersion of clay in the polymer matrix. Thinner primary particles and lower interparticle distances are obtained with the imidazolium-based MMT. This result is attributed to a higher initial gallery spacing which favors delamination phenomena. As a consequence, the dispersion state of this organoclay is much more sensitive to changes in the mixing shear rate, contrarily to the commercial ones. © 2012 Wiley Periodicals, Inc. J. Appl. Polym. Sci. 000: 000–000, 2012

KEYWORDS: nanocomposites; rheology; structure; polyethylene; organoclay

Received 16 January 2012; accepted 30 March 2012; published online
DOI: 10.1002/app.37812

INTRODUCTION

Nanocomposites constituted of a polymer matrix filled with layered silicates have attracted intensive academic and industrial interest.[1] The most commonly used layered silicate is montmorillonite (MMT). The high aspect ratio of clay nanoplatelets dispersed in the polymer phase results in a dramatic increase in interfacial area, which distinguishes this class of materials from traditional composites. Indeed, nanocomposites present enhanced properties, such as mechanical,[2–4] barrier,[2–6] and flammability resistance[7] properties, at low clay fractions. However, one of the most important criteria to achieve these improved properties is a high exfoliation degree and a good dispersion quality of clay particles in the polymer matrix. Indeed, the hydrophilic nature of the MMT surface impedes homogenous dispersion in the organic polymer phase. So, the hydrophilic MMT surface is converted to an organophilic one, exchanging metal cations present in the MMT interlayer region by cationic surfactants, usually quaternary alkyl ammonium cations. Numerous recent studies have shown that organically modified MMTs (OMMTs) can be efficiently exfoliated in polar polymers, like polyamide (PA), using appropriate melt processing techniques and optimized mixing conditions.[8–10] The average molecular weight and average molecular weight distribution of polymers may also affect the dispersion of fillers in polymer/filler nanocomposites, mainly through viscosity effects. Indeed, nanocomposites based on higher average molecular weight polyamides yield enhanced properties, due to a higher degree of clay exfoliation.[11] Polymers with a low average molecular weight, that is, a low viscosity, easily penetrate the galleries of clay platelets and promote the filler wetting, whereas a higher polymer viscosity hinders the intercalation of polymer chains between clay layers, but favors the breaking-up of primary clay particles, due to strong shear during mixing, leading to a good state of dispersion of fillers.

However, it is well-known that the high level of layered silicate exfoliation achievable with polar polymers by melt blending is hardly obtained with the more commonly used polyolefins, such as polypropylene (PP) or polyethylene (PE). Indeed, exfoliation of clay in PP or PE matrix, which are highly hydrophobic materials, is difficult because of weak interactions between the apolar polymer matrix and the polar surface of the clay. At the present time, the most promising strategy is to incorporate into

the composite a compatibilizer, that is, a small amount of a maleic anhydride grafted polyolefin, miscible with the polyolefin matrix. However, elaboration of polyolefin-based nanocomposites is a very complex challenge, even when using a compatibilizer. Indeed, graft ratio and average molecular weight of the compatibilizer,[12,13] as well as compatibilizer/clay weight ratio[14–16] play a key role in the final structure and resulting physical properties of the nanocomposite. It was also shown that the design of mixing device [17] and mixing procedures[9,18,19] affected clay dispersion within the matrix and properties of the final product. This approach, requiring a compatibilizer as third phase, has been very well-developed for PP-based nanocomposites, including some commercial applications, but not so far developed for PE systems. However, some studies, focusing on PE/compatibilizer/OMMT systems, attempt to correlate the clay structure state to macroscopic properties, such as mechanical and barrier properties.[14,17,19–22]

The nature of surfactant also plays a key role in the preparation of polymer/layered silicate nanocomposites. First, it was shown that PE nanocomposites, derived from organoclay having two alkyl tails, exhibited a better dispersion than PE nanocomposites, based on organoclay having only one tail.[14] Consequently, increasing the number of alkyl tails should lead to a better dispersion of organoclay in PE, therefore to improved macroscopic properties, whereas observations are opposite for nanocomposites based on polar polymer matrices such as PA for instance. Second, increasing the thermal stability of organically modified layered silicates is another key point in the successful elaboration of polymer/layered silicate nanocomposites on an industrial scale. Indeed, the thermal degradation of MMT modified by long chain alkyl quaternary ammonium ions begins generally at 180°C as shown by Xie et al.,[23] leading to polymer/OMMT nanocomposites with poor macroscopic properties, such as mechanical, impact,[24] and rheological[25] properties. Imidazolium salts as organomodifiers are known to have a good thermal stability, and MMT clay treated with imidazolium salts were shown to have improved thermal stability compared to MMT treated with quaternary alkyl ammonium cations.[26] The thermal degradation of MMT modified by imidazolium was shown to occur above 220°C.[27] Using ionic liquids based on imidazolium salts are therefore expected to be a promising new alternative to ammonium salts for the preparation of polymer/layered silicate nanocomposites by melt blending.

Polymer/imidazolium-based OMMT nanocomposites, without compatibilizer, were studied in terms of impact of this thermally resistant ionic liquid on the dispersion of clay in the matrix, in particular when the matrix is poly(ethylene terephthalate) (PET).[28,29] To our knowledge, only a recent paper focuses on the effect of the imidazolium ionic liquid used as surfactant on thermal and mechanical properties of PE/imidazolium-based OMMT nanocomposites.[27] Properties, more particularly for unwashed clay, are comparable with those of PE/compatibilizer/ammonium-based OMMT nanocomposites, processed with large amounts of maleic anhydride grafted PE compatiblizer.[17,19] From a processing point of view, the effect of melt-processing conditions on the dispersion quality of imidazolium treated MMT clay was only studied in the case of PET matrix.

Wide-angle X-ray diffraction (WAXD), transmission electron microscopy (TEM), and more recently atomic force microscopy (AFM) are investigation techniques which are known to be of major interest in characterizing the structure and dispersion of organoclay in polymer nanocomposites, even though they have some limitations. WAXD was found to be useful to detect clay exfoliation or intercalation, but is limited because of clay dilution, preferred orientation, and other peak broadening factors.[30] TEM and AFM techniques are local techniques, but allowing to describe clay dispersion, qualitatively and quantitatively. Indeed, the clay exfoliation degree can be evaluated through the concept of specific particle density,[11] and a clay characteristic dimension can be measured, though it is usually underestimated.[31] Rheology is a powerful indirect structural investigation technique, insofar it is highly sensitive to the clay exfoliation degree and dispersion state. Moreover, among various macroscopic material properties, melt-state rheological properties have a great interest regarding not only the study of structure/behavior relationships but also processibility. Numerous experimental studies on linear viscoelastic behavior of layered silicate nanocomposites showed the existence of a transition from liquid-like behavior to solid-like behavior, at a low silicate volume fraction ϕ_p. The behavior change has been attributed to the formation of a three-dimensional (3D) percolated network at very low clay fractions, due to the large aspect ratio of clay particles. For well-exfoliated nanocomposites, such as PA/OMMT nanocomposites, ϕ_p ranges from 1 to 2%.[25,32,33] Similar ϕ_p value was obtained for PE/compatibilizer/OMMT nanocomposites, with a compatibilizer/OMMT ratio equal to 3,[13] but, to our knowledge, no rheological investigation was ever reported in the literature for PE/imidazolium-based MMT composites, without compatibilizer.

So, the main objective of the present work was to investigate the effect of clay fraction, mixing conditions and PE matrix average molecular weight on the structure and rheological behavior of PE/imidazolium-based MMT composites, aiming at comparing them to those of PE/commercial ammonium-based MMT microcomposites.

EXPERIMENTAL

Materials

Composites were prepared from two commercial linear low density PE, the Flexirene MR 50 A, denoted PE_1, and the Flexirene FG 20F, denoted PE_2, supplied by Polimeri Europa and Enichem, respectively. Table I shows some of their characteristics, including the melting point, denoted T_m, the specific gravity, denoted ρ, the number average molecular weight, denoted M_n, and the polydispersity index, denoted I. The number average molar mass was shown to be 21,200 g/mol for PE_1, corresponding to a degree of polymerization of about 750 and a radius of gyration of 3.9 nm. For PE_2, the number average molar mass was shown to be 37,000 g/mol, corresponding to a degree of polymerization of about 1320 and a radius of gyration of 5.1 nm. Polydispersity indexes were shown to be 2.5 and 3.8, for PE_1 and PE_2, respectively. With such molecular characteristics, the PE_2 chains are expected to be more entangled than the PE_1 ones. The Newtonian viscosity, η_0, and the plateau modulus, G_0^N (*Cf.* Figure 10), measured at $T = 130$°C, are reported in

Table I. Physical Properties of Polyethylene Matrices

PE	ρ (g/cm^3)	T_m (°C)[a]	M_n (g/mol)	I	η_0 (Pa.s)[b]	G_0^N (Pa)[b]
PE_1	0.94	125	21,200	2.5	1150	3×10^5
PE_2	0.92	121	37,000	3.8	27,000	7×10^5

[a]Melt peak temperature measured by DSC at 10°C/min under nitrogen flow, [b]Rheological values measured at 130°C.

Table I, for each extruded PE. The average molecular weight between entanglements, M_e, has been calculated from the rubber elasticity model[34]:

$$M_e = \rho RT/G_0^N \quad (1)$$

leading to a number of entanglements per PE_1 chain of $\sim$ 5 and a number of entanglements per PE_2 chain six times higher.

Three types of clay were used in this work: two commercial ammonium-modified MMT, referenced as Cloisite C30B and Cloisite C20A, supplied by Southern Clay Products (Gonzales, TX) and an imidazolium modified MMT. The characteristic dimensions of an individual silicate layer are length $L \sim 200$ nm[35] and thickness $e_0 \sim 0.7$ nm, corresponding to an average aspect ratio of about 285. For C30B, C20A and C_{im} clays, interlayer gallery spacing values were calculated subtracting the thickness of the inorganic platelet from the d_{001} spacing (inter-reticular distance), determined using Bragg's law with diffraction peak angle. C30B is a methyl bis-2-hydroxyethyl tallow ammonium exchanged MMT clay. This organoclay with a single alkyl tail has an inter-reticular distance of 1.9 nm, corresponding to an interlayer gallery spacing of $\sim$ 1.2 nm, and a specific gravity of $\sim$ 2 g/cm^3. C20A is a dimethyl bis-hydrogenated-tallow ammonium exchanged MMT clay. This organoclay with two alkyl tails has an inter-reticular distance of 2.4 nm, corresponding to an interlayer gallery spacing of $\sim$ 1.7 nm, and a specific gravity of $\sim$ 1.8 g/cm^3. The third clay used in the present study, denoted C_{im}, is a MMT modified with a thermally stable ionic liquid. The ionic liquid was synthetized with two long alkyl chains (in C18) based on imidazolium, denoted $C_{18}C_{18}Im$.[27] The cationic exchange protocol used is inspired from procedures built up for preparing alkylammonium modified MMTs.[36] The sodic MMT (Nanofil 757 from Süd Chemie) is dispersed in an acidic solution at 80°C in which the iodine imidazolium salt has been previously dissolved in excess (twice the MMT Cationic Exhange Capacity for optimal cationic exchange) for the exchange to take place. After 3 h of reaction, the obtained C_{im} organomodified MMT is filtered and rinsed till complete elimination of iodine ions, checked by $AgNO_3$ titration.

C_{im} presents an inter-reticular distance of 3.8 nm, corresponding to an interlayer gallery spacing of $\sim$ 3.1 nm, and a specific gravity of $\sim$ 1.84 g/cm^3. The high value of the interlayer gallery spacing of C_{im}, reported in Table II, indicates the success of ionic liquid intercalation.[27]

Blending

The clay volume fraction dependence of rheological properties was studied with PE_1-based composites prepared by melt intercalation at 190°C, 100 rpm, corresponding to an average mixing shear rate of 1570 s^{-1}, and during 2 min, using a DSM Xplore 15 cm^3 twin screw micro-compounder. Following this route, extruded samples were prepared at various clay mass fractions, ϕ, ranging from 1.5 to 10%.

Additionally, to study the influence of mixing mechanical energy on the structure of PE_1-based composites constituted of 3% clay, two other screw rotational speeds, 50 and 150 rpm, corresponding to average mixing shear rates of 785 and 2355 s^{-1}, respectively, were used.

The influence of mixing temperature was also investigated for PE_1-based composites, extruded at 1570 s^{-1} and composed of 3% clay; to do this, another mixing temperature, 130°C, was chosen.

Besides, to study the influence of mixing conditions and mixing temperature on the structure of PE_1-based composites composed of 5% clay, a few samples were prepared by melt intercalation in a Haake Rheocord internal mixer; the residence time was 6 min and the average mixing shear rate, corresponding to the imposed rotational speed of 100 rpm, was $\sim$ 100 s^{-1}, as estimated from the model by Bousmina et al.[37] It is worth noticing that the shear rate is lower in the internal mixer than in the twin screw micro-compounder.

Finally, to study the role played by the PE matrix, a PE_2-based composite with 3% C_{im} clay was extruded at 190°C and 1570 s^{-1}.

All samples were pelletized and processed by compression molding at 190°C to get 2 mm thick plates.

Characterization Techniques

WAXD experiments were performed at ambient temperature to characterize the composite structure. X-ray diffraction patterns have been collected on a Philips Xpert MPD Pro diffractometer (40 kV, 40 mA), equipped with a graphite mono-chromatized Cu Kα1 radiation (λ = 1.5406 Å), with a scanning rate of 2 s/step, and 0.01° 2θ step size.

The morphology of composite samples was determined by TEM. Ultrathin sections were prepared at −140°C with an ultracut EM FC6 ultracryomicrotome (LEICA) using a diamond knife. Imaging was performed with a JEOL JEM-1230 at 80 kV.

Linear shear oscillatory measurements were performed using a controlled stress rheometer (GEMINI from Malvern Instruments) equipped with parallel disks of 25 mm diameter and 2 mm spacing. All samples were characterized at 130°C and all measurements performed with GEMINI rheometer were

Table II. Interlayer Gallery Spacing of OMMT and Corresponding 3 wt % PE Composites

Clay powder	C30B	C20A	C_{im}	C_{im}
d (nm)	1.2	1.7	3.1	3.1
Composite	PE_1/C30B	PE_1/C20A	PE_1/C_{im}	PE_2/C_{im}
d (nm)	1.0	2.4	3.1	3.1

performed under nitrogen. Rheometrical data were shown to be reproductible within ±5%.

RESULTS AND DISCUSSIONS

Structure

Figures 1(a–c) show TEM micrographs of PE_1 matrix composites filled with 3% C30B, C20A, and C_{im}, respectively. Composites were extruded at 1570 s^{-1} and 190°C. C30B particles are stacked in micrometric aggregates, typical of a microcomposite structure. Indeed, the presence of stacks with a length ~ 5 μm and a thickness ~ 1 μm is evidenced in Figure 1(a). Knowing the C30B inter-reticular distance, ~ 2 nm, and given a thickness of 1 μm, the number of stacked clay layers can be inferred: it is ~ 500. Figure 1(a) clearly shows large C30B aggregates, with a low average aspect ratio, poorly dispersed within PE_1 matrix. C20A clay is slightly better dispersed since the aggregates observed in Figure 1(b) are smaller than those in Figure 1(a). However, the aggregates have a rather large thickness and are still poorly dispersed within the polymer matrix. Compared to C30B or C20A aggregates, shorter and thinner C_{im} clay entities are observed, with a maximum thickness of 100 nm [Figure 1(c)] corresponding to ~ 25 stacked clay layers (C_{im} inter-reticular distance ~ 4 nm). In other words, PE_1/ C_{im} system exhibits a finer dispersion, even if its specific particle density, that is the average number of particles per μm^2 divided by the weight percent clay fraction, D ~ 0.15 particle/μm^2, is very low. Indeed, the specific particle density of PE_1/C_{im} nanocomposite is three times higher than that of PE_1/C20A, and six times higher than that of PE_1/C30B composites. The specific particle density was determined from the observation of about 100 clay entities. Moreover, the average aspect ratio seems to be higher for C_{im} clay particles than for C30B or C20A particles, mainly because of the presence of some rather long, ~ 2 μm, C_{im} clay particles, as shown in Figure 1(c). All those results would tend to suggest that the larger interlayer gallery spacing of C_{im} clay particles might help the delamination of C_{im} clay aggregates. Nevertheless, it is worth noticing that the dispersion level of PE_1/C_{im} nanocomposites is very low compared to that of partially exfoliated PA/C30B nanocomposites.[11,25]

Figure 2(a,b) show TEM micrograph of PE_1 matrix composites at 3% C_{im} loading. TEM micrograph of the nanocomposite extruded at 2355 s^{-1} and 190°C [Figure 2(a)] illustrates the influence of average mixing mechanical energy on the structure of PE_1/C_{im} nanocomposite. The increase of mixing shear intensity favors the delamination of clay aggregates, leading to longer and thinner clay entities, that is, with a higher aspect ratio [Figure 2(a)], which is accompanied by a slight increase of specific particle density (D ~ 0.2 particle/μm^2). Globally, the nanocomposite, extruded at 2355 s^{-1} and 190°C, exhibits a finer dispersion of C_{im} clay particles, with an aspect ratio significantly higher than that of clay entities of nanocomposite extruded at 1570 s^{-1} and 190°C [Figure 1(c)].

The effect of mixing temperature on the structure is shown in Figure 2(b), for a PE_1/C_{im} nanocomposite, extruded at 1570 s^{-1} and at a low mixing temperature of 130°C. The sample is mainly composed of short C_{im} clay particles (length ~ 500 nm), with an increased specific particle density, D ~ 0.3 particle/μm^2. The better dispersion of clay when decreasing temperature could be explained by the lower viscosity of the matrix, which enhances the efficiency of mixing shear, reinforcing the phenomenon of delamination, which leads to the breaking-up of clay aggregates. This viscosity effect is confirmed by the results presented in Figure 2(c), which shows a typical TEM

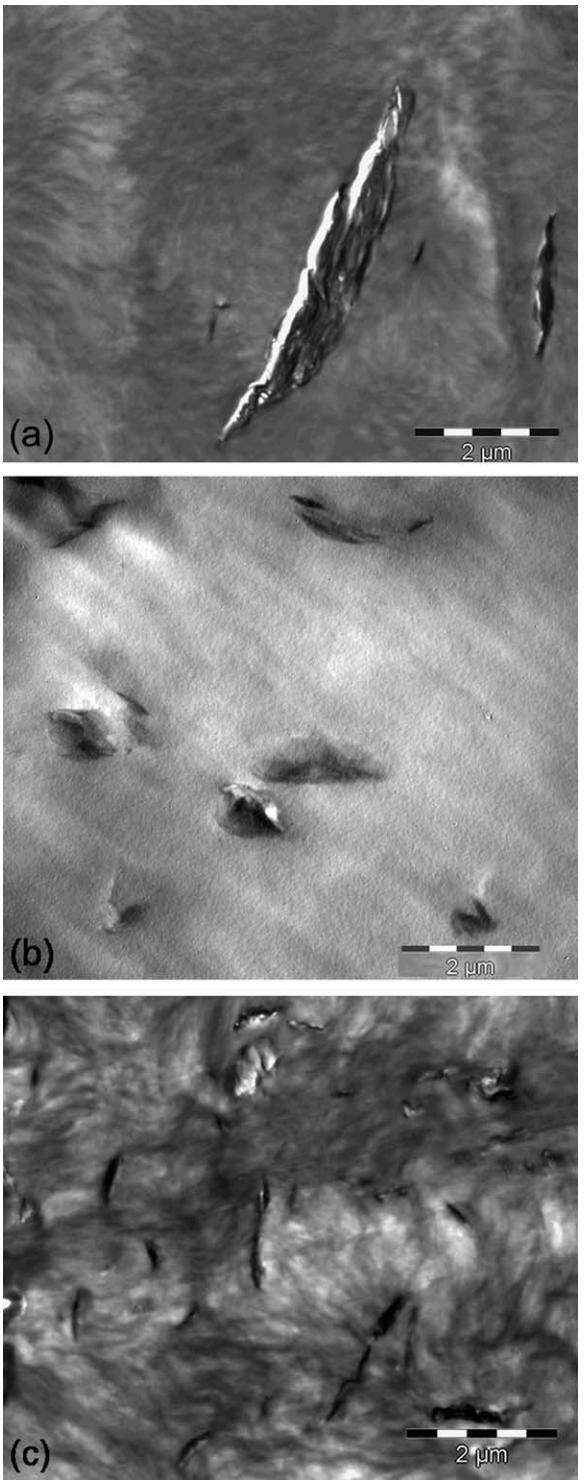

Figure 1. TEM micrographs of PE_1 composites processed at 1570 s^{-1}, 190°C containing 3 wt % of C30B (a), C20A (b) and C_{im} (c).

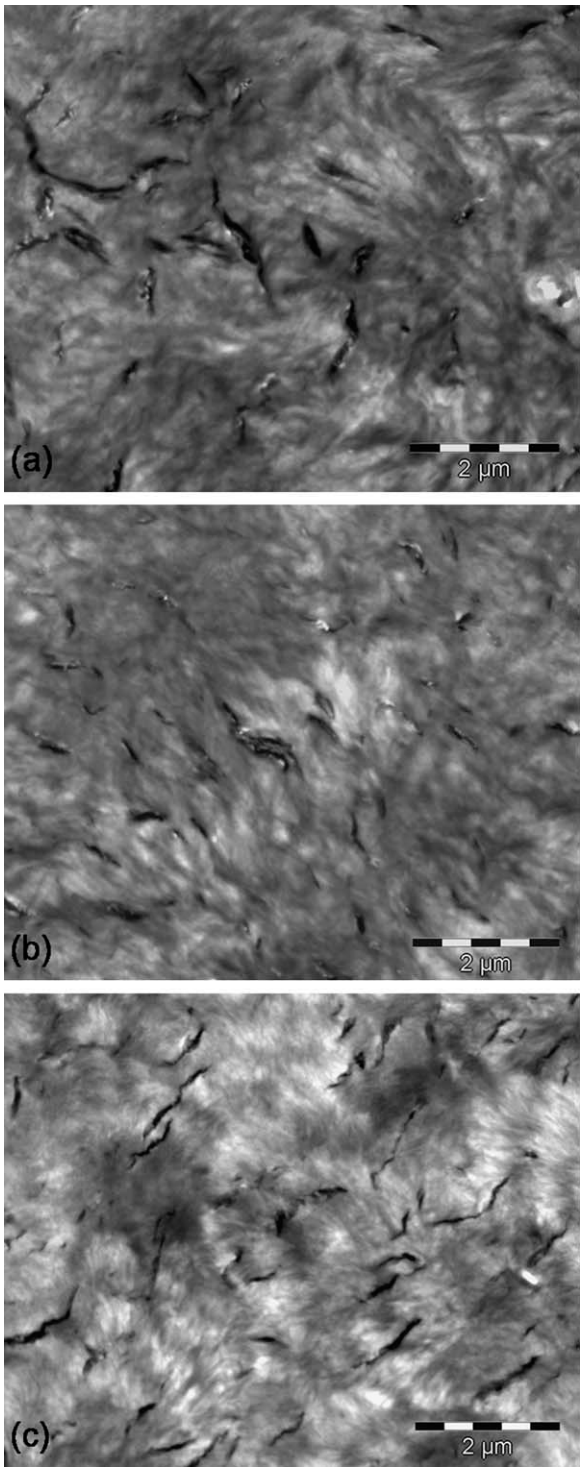

Figure 2. TEM micrographs of PE_1/C_{im} (3 wt %) nanocomposites processed at 2350 s^{-1}, 190°C (a), 1570 s^{-1}, 130°C (b), and of PE_2/C_{im} (3 wt %) nanocomposite processed at 1570 s^{-1}, 190°C (c).

micrograph of PE_2 matrix composite filled with 3% C_{im}, extruded at 1570 s^{-1} and 190°C. The structure of PE_2 nanocomposite, based on the more viscous PE matrix, is composed of numerous long C_{im} clay entities, as already observed for the PE_1 nanocomposite extruded at 2355 s^{-1} and 190°C. Moreover, both nanocomposites have the same specific particle density ($D \sim 0.2$ particle/μm^2), that is the same degree of dispersion. This result confirms that, in addition to mixing shear intensity, the level of PE matrix viscosity plays a key role in the breaking-up of C_{im} clay aggregates.

Interlayer gallery spacings of C30B, C20A, C_{im} and their corresponding composites at 3% clay loading, extruded at 1570 s^{-1} and 190°C were measured by wide angle X-ray diffraction technique and reported in Table II. The diffraction peak of PE_1/C30B composite is barely shifted to a higher diffraction angle, corresponding to an interlayer gallery spacing of ~ 1 nm. The slight decrease of interlayer gallery spacing was already observed and described.[38,39] An increase in interlayer gallery spacing is obtained when C20A is mixed with the PE1 matrix, which could suggest that PE chains have intercalated this more apolar organoclay. However, it is worth noticing that the increase of interlayer gallery spacing, relative to neat C20A, is moderate, that is ~ 40%. More interestingly, it can be noticed that the gallery spacing of C20A is still smaller than that of C_{im} clay.

Besides, the influence of molecular characteristics of PE matrix and mixing conditions on the structural state of C_{im} clay, presenting the higher interlayer gallery spacing, was investigated. the diffraction peak of C_{im} clay, PE_1/C_{im} and PE_2/C_{im} composites appeared at the same angle, $2\theta = 2.2°$, meaning that the interlayer gallery spacing, ~ 3.1 nm, was not dependent on PE molecular characteristics (Table II). As far as PE_1 matrix is concerned, the radius of gyration being close to the interlayer gallery spacing of C_{im} clay, the PE chains are not expected to affect the clay structure. Concerning PE_2, which have a radius of gyration larger than the interlayer gallery spacing of C_{im} clay, the absence of modification of clay structure means that the PE_2 chains are not intercalated within clay galleries.

Finally, wide angle X-ray diffraction results (not shown here) proved that the interlayer gallery spacing of PE_1/C_{im} nanocomposites, ~ 3.1 nm, was not influenced by mixing conditions. The absence of influence of mixing conditions on interlayer gallery spacing underlines the limited efficiency of the mixing process for PE/C_{im} nanocomposites. Indeed, mixing leads to partial shear-induced delamination of large aggregates, but cannot modify the interlayer spacing, which prevents from complete delamination, that is from exfoliation of the primary clay particles.

Viscoelastic Properties

Effect of Clay Fraction. First of all, for the highest concentration of $C_{18}C_{18}Im$ used in this work, that is, 2.5%, the linear viscoelastic behavior of $PE_1/C_{18}C_{18}Im$ blend was found (not shown here) to be quite similar to that of the PE_1 matrix, in the terminal relaxation zone. So, it can be concluded that possible interactions between the $C_{18}C_{18}Im$ ionic liquid and the PE have no measurable effects on the rheology of the PE_1 matrix at low frequencies. Consequently, rheological behaviors, described below, will be attributed to C_{im} clay fraction effects.

Strain sweep experiments were first conducted, at a fixed frequency of 1 Hz, to determine the extent of the linear viscoelastic regime. Figure 3 shows the extent of the linear response

Applied Polymer SCIENCE

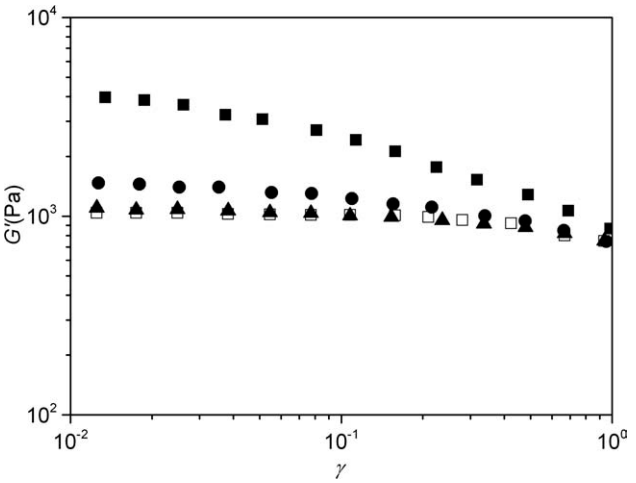

Figure 3. Storage modulus at 130°C as a function of strain for PE_1/C_{im} nanocomposites mixed at 1570 s^{-1} and 190°C: □ $\phi = 0\%$, ▲ $\phi = 3\%$, • $\phi = 5\%$, and ■ $\phi = 10\%$.

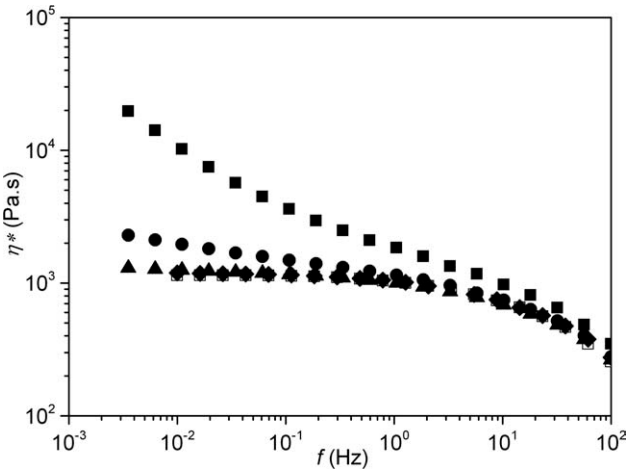

Figure 4. Complex viscosity at 130°C as a function of frequency for PE_1/C_{im} nanocomposites mixed at 1570 s^{-1} and 190°C: □ $\phi = 0\%$, ◆ $\phi = 1.5\%$, ▲ $\phi = 3\%$, • $\phi = 5\%$, and ■ $\phi = 10\%$.

regime determined from G' plots, for PE_1/C_{im} nanocomposites extruded at 1570 s^{-1} and 190°C.

The critical strain, γ_c, of all systems prepared under these mixing conditions is reported in Table III. The critical strain is about 40% for PE matrix, and is sensitive to the amount of clay: nonlinearities appear at lower strain values as the clay fraction increases. This effect is less pronounced for the PE_1/C30B microcomposite and very marked for the PE_1/C_{im} nanocomposite, for which clay particle interactions are stronger, just because clay particles are closer [Figure 1(a,c)].

Figure 4 shows the complex viscosity, η^*, as a function of frequency, for PE_1/C_{im} nanocomposites extruded at 1570 s^{-1} and 190°C. At low frequencies and below 5% clay mass fraction, the complex viscosity exhibits a plateau, defining a Newtonian viscosity η_0^*. For the 10% clay mass fraction, the slope of the complex viscosity curve, close to −1 at low frequencies, is indicative of a yield behavior. Such a yield behavior is always observed for nanocomposites as soon as interparticulate interactions become important and form a percolated 3D network, but it may appear at much lower clay loadings, for example at ∼ 1.5% [25] for well-exfoliated PA layered silicate nanocomposites.

For all PE_1/clay composites, prepared at 1570 s^{-1} and 190°C and exhibiting a Newtonian behavior, the relative Newtonian viscosity, η_{0r}, ratio of the Newtonian viscosity of composite to that of the PE_1 matrix, is displayed as a function of clay volume fraction, Φ, in Figure 5. In the dilute regime, these results were discussed in terms of intrinsic viscosity $[\eta]$, determined by fitting the curve to the second-order Einstein-type eq. (2):

$$\eta_{0r} = 1 + [\eta]\Phi + k([\eta]\Phi)^2 \quad (2)$$

where k is an interaction constant

Knowing the intrinsic viscosity, the aspect ratio, $p = L/e$ (diameter/thickness), of the disk-like clay particles can be inferred[32]:

$$[\eta] = 2.5 + 0.025(1 + p^{1.47}) \quad (3)$$

Intrinsic viscosity, $[\eta]$ and interaction constant, k, as well as aspect ratio, p, of clay entities are reported in Table IV. The volume fraction of freely rotating disks is $3/2p$ times the volume

Table III. Critical Strain, γ_c at 130°C, Versus Clay Mass Fraction, for Nanocomposites Mixed at 1570 s^{-1} and 190°C

	ϕ = 3%	ϕ = 5%	ϕ = 10%
PE_1/C30B	40%	40%	30%
PE_1/C20A	40%	30%	10%
PE_1/C_{im}	40%	10%	3%

Fillers are C30B, C20A, or C_{im}.

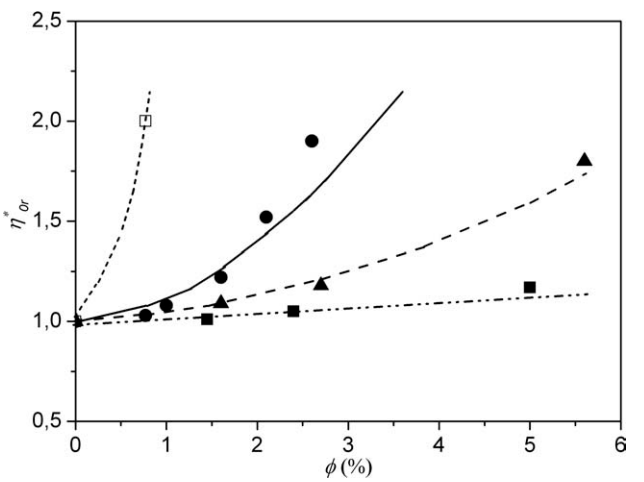

Figure 5. Relative Newtonian viscosity at 130°C as a function of organoclay volume fraction for PE_1/organoclay composites mixed at 1570 s^{-1} and 190°C: ■ C30B, ▲ C20A and • C_{im}. □ Relative Newtonian viscosity at 200°C of PA/C30B nanocomposite mixed at 200°C and 50 s^{-1} during 6 min.[33] Lines correspond to eq. (2) with: ·–·– $[\eta] = 2.5$, $k = 0$; – – – $[\eta] = 3$, $k = 20$; —— $[\eta] = 5$, $k = 35$; ---- $[\eta] = 100$, $k = 0.5$.[33]

Table IV. Intrinsic Viscosity, [η], and Interaction Constant, k, from eq. (2), Aspect Ratio, p, of Clay Entities from eq. (3), for PE_1/Clay Composites

	[η]	k	p
C30B	2.5	0	1
C20A	3	20	7
C_{im}	5	35	23

fraction of equivalent hard spheres. Assuming a critical volume fraction of spheres at percolation to be ~ 30%, the freely rotating disk-like clay particles are expected to percolate at a critical volume fraction of ~ 45, 6.1, and 1.9% for C30B, C20A, and C_{im}, respectively. Although the experimental results plotted in Figure 5 cannot confirm the calculated values of the percolation threshold, they tend to exhibit the same trends. These results deduced from rheological measurements clearly evidence differences in structure between the three composites: PE_1/C30B is a microcomposite, whereas PE_1/C_{im} can be considered as a nanocomposite, as suggested by TEM observation [Figure 1(a,c)]. However, compared to PA-12/C30B nanocomposites,[25] Figure 5 shows that PE_1/C_{im} is a non-exfoliated nanocomposite, as suggested by TEM micrographs [Figure 1(c)] and X-ray diffraction results.

Figure 6 shows the storage modulus as a function of frequency in the linear viscoelastic domain. Results show that, as far as the low-frequency zone is concerned, storage modulus gradually increases with clay content. For the sample filled with 10 wt % C_{im}, a marked low-frequency plateau storage modulus, G_0', characteristic of a pseudo-solid behavior,[25] is observed. However, at high frequencies, there is no significant effect of clay content: all G' curves are close to that of the PE matrix, contrary to what has been observed by Lim and Park[40] for exfoliated clay/PEgMA nanocomposites. The increase of G' at low frequency, which is representative of a better organoclay dispersion state, is similar to what was obtained by Durmus et al.[13] when using an oxidized PE as a compatibilizer, but is less marked than that obtained when using a maleic anhydride grafted PE.

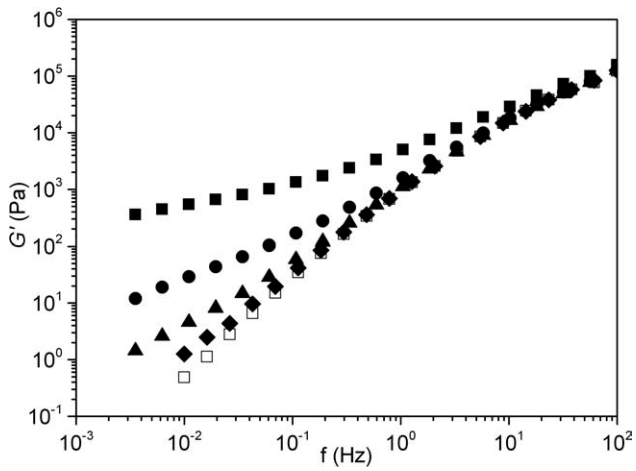

Figure 6. Storage modulus at 130°C as a function of frequency for PE_1/C_{im} nanocomposites mixed at 1570 s^{-1} and 190°C: □ ϕ = 0%, ◆ ϕ = 1.5%, ▲ ϕ = 3%, ● ϕ = 5% and ■ ϕ = 10%.

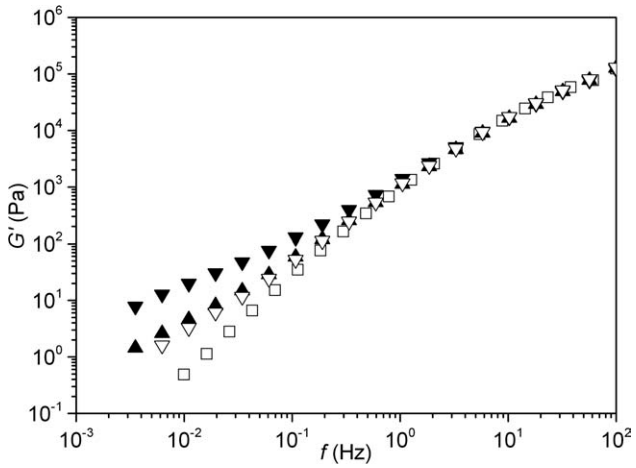

Figure 7. Storage modulus at 130°C as a function of frequency for PE_1 (□) and PE_1/C_{im} (3 wt %) nanocomposites mixed at 190°C: ▽ 785 s^{-1}, ▲ 1570 s^{-1}, and ▼ 2355 s^{-1}.

Effect of Processing Conditions. Effects of mixing shear rate and mixing temperature on storage modulus of PE_1/C_{im} nanocomposite with 3% clay are shown in Figures 7 and 8, respectively. At low frequencies, the storage modulus increases with increasing screw rotational speed (Figure 7), that is, with increasing mixing shear rate. Nevertheless, a mixing shear rate, between 1570 and 2355 s^{-1} in this study, is needed to obtain a significant increase of low-frequency storage modulus. The material extruded at the higher mixing shear rate (2355 s^{-1}) is a nanocomposite composed of thin and/or long clay entities [Figure 2(a)], well-dispersed within the PE_1 matrix.

The low frequency storage modulus also increases with decreasing mixing temperature (Figure 8). In the study, the increase of PE_1 matrix viscosity, due to the decrease of mixing temperature (130°C), leads to a finer clay dispersion [Figure 2(b)], and

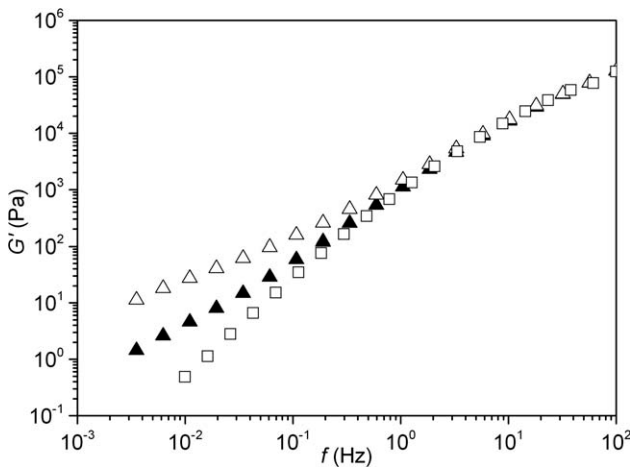

Figure 8. Storage modulus at 130°C as a function of frequency for PE_1 (□) and PE_1/C_{im} (3 wt %) nanocomposites mixed at 1570 s^{-1}: ▲ T = 190°C and △ T = 130°C.

Applied Polymer SCIENCE

therefore a higher storage modulus at low frequencies, $G' > 10$ Pa at ~ 0.03 Hz (Figure 8). However, it is worth noticing that, at this frequency, the storage modulus is about hundred times lower than that for partially exfoliated PA/C30B nanocomposites.[25]

Those results show that processing conditions play a key role in obtaining a fine dispersion of clay nanoparticles within PE matrix. The decrease of mixing temperature and the increase of mixing shear rate clearly improve the reduction in size of C_{im} clay entities [Figures 1(c) and 2(a,b)], through delamination mechanisms, but nevertheless do not lead to the intercalation of PE chains into clay galleries, which makes exfoliation of primary clay entities impossible.

Figure 9 presents the storage modulus as a function of frequency for samples prepared at 5% C_{im} clay under different mixing conditions. These results confirm trends and amplify effects previously described for the 3% clay fraction. Indeed, at 5% C_{im} clay fraction, the low frequency storage modulus also increases with (i) increasing mixing shear rate and (ii) decreasing mixing temperature. Moreover, the PE_1/C_{im} nanocomposite, extruded at 2355 s^{-1} and 130°C, exhibits a very marked low-frequency plateau storage modulus, $G'_0 \sim 100$ Pa. This value is 10 times higher than the low-frequency plateau storage modulus value measured for the nanocomposite filled with 5% C_{im} and extruded at 1570 s^{-1} and 190°C (Figure 6).

It is worth noticing that this effect of processing conditions has not been observed when using C30B or C20A OMMT. C20A is chemically very similar to C_{im} with two alkyl tails on a cationic head, but its dispersion does not depend on the mixing shear rate, at least at the shear rate used in this study, probably because the gallery size of C20A clay is not high enough to allow efficient delamination of clay aggregates.

Effect of Matrix. Figure 10 shows the influence of the average molecular mass of the PE matrix on the storage modulus PE-based nanocomposites. Classical effects, such as the increase of low-frequency storage modulus observed for PE_1/C_{im} nanocomposites, are not observed in the case of PE_2/C_{im} nanocomposites in the range of frequencies studied, despite a better state of dispersion [cf., Figure 1(c) compared to Figure 2(c)] under the same processing conditions. Actually, interparticulate interactions are probably somewhat masked by the contribution of the high PE_2 matrix viscosity at low frequencies, which could explain the absence of apparent yield stress (solid-like) behavior in PE_2 based nanocomposites, as suggested by Carreau and Lavoie[41] when discussing the rheological properties of filled polymers.

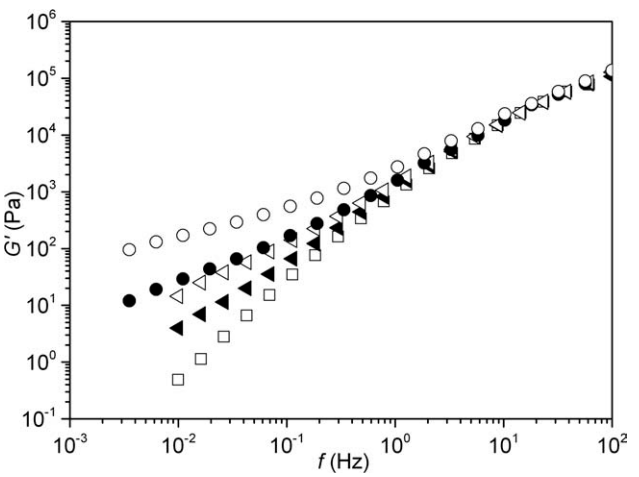

Figure 9. Storage modulus at 130°C as a function of frequency for PE (□) and PE_1/C_{im} (5 wt %) nanocomposites mixed at: ◀ 190°C and 100 s^{-1}, using the internal mixer; ◁ 130°C and 100 s^{-1}, using the internal mixer ● 190°C and 1570 s^{-1}, using the twin screw micro-compounder ○ 130°C and 2355 s^{-1}, using the twin screw micro-compounder.

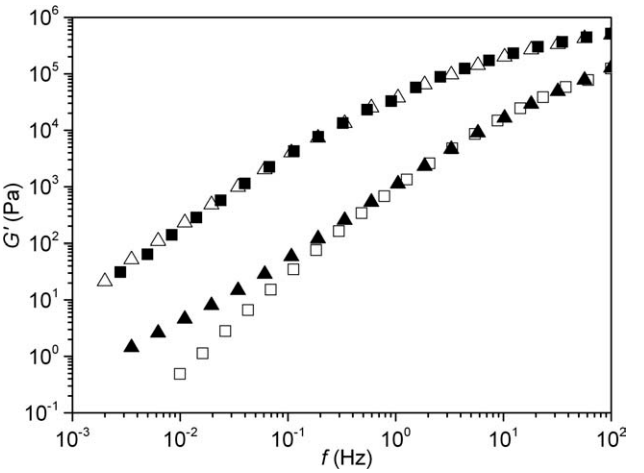

Figure 10. Storage modulus at 130°C as a function of frequency for PE_1 (□), PE_2 (■), PE_1/C_{im} (▲) and PE_2/C_{im} (△) nanocomposites, filled with 3 wt % clay and mixed at 1570 s^{-1} and 190°C.

CONCLUSION

In this study, we first evidenced, through rheological characterization and TEM observations, that using MMT modified with imidazolium ionic liquids instead of traditional commercial organoclays, namely Cloisite, can help obtaining PE-based nanocomposites, exhibiting a good state of dispersion without using any compatibilizer.

Besides, the results highlight the difference in degree of dispersion between the various clay particles studied: the imidazolium OMMT particles are at least three times thinner and closer from each other than their alkylammonium equivalents, when dispersed under the same processing conditions. Moreover, we also evidenced that, due to a very high initial gallery spacing, the state of dispersion of the imidazolium OMMT was particularly sensitive to the mixing shear rate. The initial very high interlayer gallery spacing of this imidazolium-based organoclay facilitates the partial delamination of clay particles. Lowering the mixing temperature or increasing the average shear rate during the mixing process improves the degree of dispersion; however, as PE chains do not penetrate through clay galleries, complete delamination, that is exfoliation, is impossible, contrary to what can be obtained with PA-based nanocomposites.

ACKNOWLEDGMENTS

The authors thank P. Roquefort for preparing PE/clay composites, P. Babin and A. Gosnet from CERDATO Arkema (Serquigny, France) for performing TEM observations, R. Retoux, X. Larose and G. Renouf from CRISMAT laboratory (UMR6508, Caen, France) for additional TEM observations, M. Boisserie from CIMAP laboratory (UMR6252, Caen, France) for performing XRD experiments as well as P. Bas and L.-M. Grand who processed some composites during their undergraduate lab project. This work has been performed within the "PUNCHOrga" (Pôle Universitaire de Chimie Organique) and the "RMPP" (Réseau Matériaux, Polymères, Plasturgie) interregional networks. They gratefully aknowledge the "Ministère de la Recherche et des Nouvelles Technologies," CNRS (Centre National de la Recherche Scientifique), the "Région Basse-Normandie" and the European Union (FEDER funding) for financial support.

REFERENCES

1. Ray, S. S.; Okamoto, M. *Prog. Polym. Sci.* **2003,** *28*, 1539.
2. Alexandre, M.; Dubois, P. *Mat. Sci. Eng.* **2000,** *28*, 1.
3. Le Pluart, L., Duchet, J.; Sautereau, H. *Polymer* **2005,** *46*, 12267.
4. Aït-Hocine, N., Médéric, P.; Aubry, T. *Polym. Test.* **2008,** *27*, 330.
5. Osman, M. A., Mittal, V., Morbidelli, M.; Suter, U. W. *Macromolecules* **2003,** *36*, 9851.
6. Alexandre, B., Langevin, D., Médéric, P., Aubry, T., Couderc, H., Nguyen, Q. T., Saiter, A.; Marais, S. *J. Membrane Sci.* **2008,** *328*, 186.
7. Gilman, J. W., Jackson, C. L., Morgan, A. B., Harris, R., Manias, E.; Giannelis, E. P. *Chem. Mater.* **2000,** *12*, 1866.
8. Dennis, H. R., Hunter, D. L., Chang, D., Kim, S., White, J. L., Cho, J. W.; Paul, D. R. *Polymer* **2001,** *42*, 9513.
9. Lertwimolnun, W.; Vergnes, B. *Polym. Eng. Sci.* **2007,** *47*, 2100.
10. Médéric, P., Aubry, T.; Razafinimaro, T. *Int. Polym. Proc.* **2009,** *24*, 261.
11. Fornes, T. D., Yoon, P. J., Keskkula, H.; Paul, D. R. *Polymer* **2001,** *42*, 9929; Erratum: *Polymer* **2002,** *43*, 2121–2122.
12. Hasewaga, N., Kawasumi, N., Kato, M., Usuki, A.; Okada, A. *J. Appl. Polym. Sci.* **1998,** *67*, 87.
13. Durmus, A., Kasgoz, A.; Macosko, C. *Polymer* **2007,** *48*, 4492.
14. Hotta, S.; Paul, D. R. *Polymer* **2004,** *45*, 7639.
15. Wang, Y., Chen, F. B.; Wu, K. C. *J. Appl. Polym. Sci.* **2005,** *97*, 1667.
16. Chissopoulou, K., Altintzi, I., Anastasiadis, S. H., Giannelis, E. P., Pitsikalis, M., Hadjichristidis, N.; Theophilou, N. *Polymer* **2005,** *46*, 12440.
17. Lotti, C., Isaac, C. S., Branciforti, M. C., Alves, R. M. V., Liberman, S.; Bretas, R. E. S. *Eur. Polym. J.* **2008,** *44*, 1346.
18. Liang, G., Xu, J., Bao, S.; Xu, W. *J. Appl. Polym. Sci.* **2004,** *91*, 3974.
19. Filippi, S., Marazzati, C., Magagnini, P., Famulari, A., Arosio, P.; Meille, S. V. *Eur. Polym. J.* **2008,** *44*, 987.
20. Kato, M., Okamoto, H., Hasegawa, N., Tsukigase, A.; Usuki, A. *Polym. Eng. Sci.* **2003,** *43*, 1312.
21. Lee, J. H., Jung, D., Hong, C. E., Rhee, K. Y.; Advani, S. G. *Compos. Sci. Technol.* **2005,** *65*, 1996.
22. Morawiec, J., Pawlak, A., Slouf, M., Galeski, A., Piorkowska, E.; Krasnikowa, N. *Eur. Polym. J.* **2005,** *41*, 1115.
23. Xie, W., Gao, Z., Pan, W. P., Hunter, D., Singh, A.; Vaia, R. *Chem. Mater.* **2001,** *13*, 2979.
24. McNally, T., Murphy, W. R., Lew, C. Y., Turner, R. J.; Brennan, G. P. *Polymer* **2003,** *44*, 2761.
25. Médéric, P., Razafinimaro, T.; Aubry, T. *Polym. Eng. Sci.* **2006,** *46*, 986.
26. Awad, W. H., Gilman, J. W., Nyden, M., Harris Jr, R. H., Sutto, T. E., Callahan, J., Trulove, P. C., De Long, H. C.; Fox, D. M. *Thermochim. Acta* **2004,** *409*, 3.
27. Livi, S., Duchet-Rumeau, J., Pham, T. N.; Gérard, J. F. *J. Colloid. Interf. Sci.* **2010,** *349*, 424.
28. Davis, C. H., Mathias, L. J., Gilman, J. W., Schiraldi, D. A., Shields, J. R., Trulove, P., Sutto, T. E.; DeLong, H. C. *J. Polym. Sci. Pol. Phys* **2002,** *40*, 2661.
29. Monemian, S. A., Goodarzi, V., Zahedi, P.; Angajy, M. T. *Adv. Polym. Tech.* **2007,** *26*, 247.
30. Eckel, D. F., Balogh, M. P., Fasulo, P. D.; Rodgers, W. R. *J. Appl. Polym. Sci.* **2004,** *93*, 1110.
31. Picard, E., Vermogen, A., Gérard, J. F.; Espluche, E. *J. Membrane Sci.* **2007,** *292*, 133.
32. Utracki, L. A.; Lyngaae-Jorgensen, J. *Rheol. Acta.* **2002,** *41*, 394.
33. Aubry, T., Razafinimaro, T.; Médéric, P. *J. Rheol.* **2005,** *49*, 425.
34. Ferry, J. D. In Viscoelastic Properties of Polymers, 3rd ed.; Wiley: New York, **1980.**
35. Paul, D. R.; Robeson, L. M. *Polymer* **2008,** *49*, 3187.
36. Le Pluart, L., Duchet, J., Sautereau H.; Gerard, J.-F. *J. Adhesion* **2002,** *78*, 645.
37. Bousmina, M., Aït-Kadi, A.; Faisant, J. B. *J. Rheol.* **1999,** *43*, 415.
38. Galgali, G., Ramesh, C.; Lele, A. *Macromolecules* **2001,** *34*, 852
39. Wang, K. H., Choi, M. H., Koo, C. M., Choi, Y. S.; Chung, I. J. *Polymer* **2001,** *42*, 9819.
40. Lim, Y. T.; Park, O. O. *Rheol. Acta* **2001,** *40*, 220.
41. Carreau, P. J.; Lavoie, P.-A. *Macromol. Symp.* **1996,** *108*, 111.